scientific reports

Check for updates

OPEN

Influence of grain size and spatial volume fraction variation in ZnO based functionally graded thermoelectric devices

Shardul Rai[1], Kshitij Kumar Sharma[2], Abhishek Tewari[2] & Ankit Gupta[1]✉

In the present study, a novel coupled analytical - finite element model is developed to examine the effect of spatially varying volume fractions of differently sized ZnO grains on the performance of functionally graded thermoelectric devices (FGTEDs). The volume fraction distribution of grains along the device length is defined using the power's law function. The volume fraction variation parameter (*n*) is varied from 0 to ∞, and the corresponding power output of the device is systematically analysed and compared. The grain sizes ranging from 0.18 µm to 5.75 µm are considered in the temperature range 120 K to 675 K. The results indicate that the FGTEDs with a higher volume fraction of larger grains yields a greater power output. A maximum power output of 2.6341 x 10^{-4} W and a peak figure of merit of 0.006 at 345 K are achieved. Furthermore, a sensitivity analysis performed reveals that the electrical resistivity has the most significant influence on the power output, followed by the Seebeck coefficient and the thermal conductivity. This study underscores the crucial role of grain size distribution in optimizing the performance of ZnO based FGTEDs.

Thermoelectric materials or devices (TEMs/TEDs) are capable of transforming heat into electrical energy[1–4]. It was discovered by Thomas Seebeck in the year 1823[5]. TEDs have potential to harness any thermal sources including waste heat without any vibration or noise[6,7]. However, the low energy conversion efficiency restricts the areas of application to medical equipment, laboratory instruments, and space power generation, where energy availability and reliability are important over cost and efficiency[8–10].

It has been established over the years that the performance of the TEMs/TEDs is assessed using two dimensionless parameters, known as the figure of merit (*ZT*) and the thermoelectric efficiency (η)[11–16]. The major issue with the homogeneous TEMs/TEDs lies in its optimization over the applied temperature range. Certain regions get subjected to temperatures where the *ZT* falls below its maximum value. The efforts to overcome such issue has led to the development of functionally graded thermoelectric materials/devices (FGTEMs/FGTEDs).

In the FGTEMs/FGTEDs, the composition is varied intentionally in a gradual fashion throughout the volume, leading to the variation in thermoelectric properties[17–20]. Functional gradation allows operating different sections of the TEMs/TEDs in the temperature range in which its *ZT* or η is maximum[21]. It is well established that the properties of the semiconducting materials are strongly influenced by carrier concentration, which can be adjusted through suitable doping and grain size engineering[22,23]. Therefore, researchers have employed such methods for obtaining suitable thermoelectric properties in different sections of the FGTEDs while fabricating[24]. Gelbstein et al.[25] provided an overview of the design considerations, synthesis techniques, and characterization methods for graded p-type $Pb_{1-x}Sn_xTe$ samples with uniform layer widths. Dashevsky et al.[26] deliberated on the efficiency aspects within a FGTEM doped with indium in the context of PbTe. Belmonte et al.[27] proposed a one-step fabrication method for Si_3N_4 based FGTEM featuring a continuous variation in grain size. Banerjee et al.[28] reported on the fabrication of chitosan - BST composite thermoelectric films, presenting a novel method to tailor the microstructure and enhancing the *ZT*.

The potential of functional gradation has also been highlighted by some researchers through analytical studies. Mahan et al.[29] conducted a one-dimensional numerical investigation and put forward the concept of continuously altering the properties of TEMs along the length to get enhanced overall *zT*. Jin et al.[30] analytically proved that the peak η can be increased by varying the thermoelectric properties along the length, as in the case

[1]School of Engineering, Shiv Nadar Institution of Eminence Deemed to be University, Gautam Buddha Nagar 201314, India. [2]Department of Metallurgical and Materials Engineering, Indian Institute of Technology Roorkee, Uttarakhand 247667, India. ✉email: ankit.gupta1@snu.edu.in

of the FGTEDs. Cao et al.[17] analytically predicted a maximum η of around 25 % by independently varying the thermoelectric properties in the FGTEDs. It is very well known that the thermoelectric properties vary with temperature and during analytical analysis, the temperature dependency of the thermoelectric properties must be considered[31,32].

Pertaining to the high temperature thermoelectric applications, ZnO stands out as a promising material, particularly for harnessing waste heat from power plants. When compared with traditional TEMs like Bi_2Te_3, PbTe, and SiGe, ZnO is stable in much wider temperature range of 300 K - 1300 K[33]. Moreover, it is safer, affordable and less toxic as compared to other TEMs like PbTe and SnTe[34–37]. Despite of such advantages, the primary drawback is its oxide nature. The strong ionic bonds and low mass of oxygen atom leads to high vibrational frequencies resulting to undesirably high lattice thermal conductivity[38].

In the past, research on ZnO has primarily been focused on reducing its thermal conductivity. Nam et al.[39] doped ZnO with Al which caused phonon scattering resulting to reduced thermal conductivity and high *ZT* of 0.34 at 1073 K. Gautam et al.[40] obtained reduced thermal conductivity of 1 W/m/K by introducing nanocomposites in the Al-doped ZnO and reported *ZT* of 0.24 at 950 K. Ohtaki et al.[41] performed Al and Ga co-doping in ZnO and obtained high *ZT* of 0.65 at 1247 K. Tang et al.[42] introduced porosity of 35 % in Si film for phonon scattering and reported high *ZT* value of 0.4 at very low temperature of 300 K. Yang et al.[43] conducted theoretical study and showed 10^{-3} times reduction in thermal conductivity for 90 % porous Si crystal.

Explorations into experimental fabrication and analytical analysis of the FGTEMs/FGTEDs have been underway since the 1990s, but the impact of grain size gradation, particularly for ZnO based FGTEMs/FGTEDs, remains largely underexplored[44]. Cramer et al.[45] in the year 2017 fabricated a ZnO based FGTED varying the grain size from 0.18 μm at cold side to 1.2 μm at hot side. It marked the initial instance of a thermoelectric semiconductor or ceramic being subjected to such an extensive micro-structural gradation. In the context of suitable element doping, Cramer et al.[46] synthesized an Al-doped ZnO based FGTED in which the doping % varied from 0 % at hot side to 5 % at cold side and documented the maximum η of 0.24.

Research gap and novelty

The literature on ZnO based FGTEMs/FGTEDs lacks a thorough investigation into the impact of spatially varying volume fractions of ZnO grains, having different sizes, on the power output. Additionally, a systematic methodology to identify the most and the least significant thermoelectric property affecting the power output remains largely unexplored.

Therefore, the aim of the present work is to examine the impact of grain size distribution and its spatial variation on the power output. The proposed methodology includes developing a hybrid framework which combines analytical formulation with a finite element analysis model. The analytical formulation allows incorporating and optimizing the spatial volume fraction distribution of differently sized grains, while the computational model enables the evaluation of the power output. Subsequently, a comparative analysis is conducted to evaluate the performance trend.

Further, for determining the specific influence of the Seebeck coefficient (*S*), thermal conductivity (κ), and electrical resistivity (ρ) on the power output, a sensitivity analysis based on the ANOVA results is reported. To the best of the authors' knowledge, this is the first reported sensitivity analysis of its kind for ZnO based FGTEDs and is expected to serve as a benchmark for future research studies.

Temperature distribution governing equation

In the present section, the temperature distribution governing equation for a FGTED is derived and its solution is obtained by combining the finite difference method (FDM) with the Thomas algorithm method[47]. A FGTED with the Seebeck coefficienct (*S*), thermal conductivity (κ), and electrical resistivity (ρ) as functions of position (x) is presented in Fig. 1.

The foundational thermoelectric equations along x-direction are given as[17–19]

$$J=\frac{\mathrm{E}}{\rho}-\frac{\mathrm{S}}{\rho}\frac{\mathrm{dT}}{\mathrm{dx}}, \tag{1}$$

$$q=-\kappa\frac{\mathrm{dT}}{\mathrm{dx}}+STJ, \tag{2}$$

$$\frac{\mathrm{dq}}{\mathrm{dx}}=\mathrm{JE}, \tag{3}$$

$$\frac{\mathrm{dJ}}{\mathrm{dx}}=0, \tag{4}$$

$$E=-\frac{\mathrm{d}\varphi}{\mathrm{dx}}, \tag{5}$$

where, T, J, q, E, and φ represents absolute temperature, current density, heat flux, electric field, and electric potential, respectively. The limiting conditions for the temperature field are,

$$T=\mathrm{T_C},\ \text{at x}=-\frac{\mathrm{L}}{2}, \tag{6a}$$

$$T=T_H,\ \text{at}\ x=\frac{L}{2} \tag{6b}$$

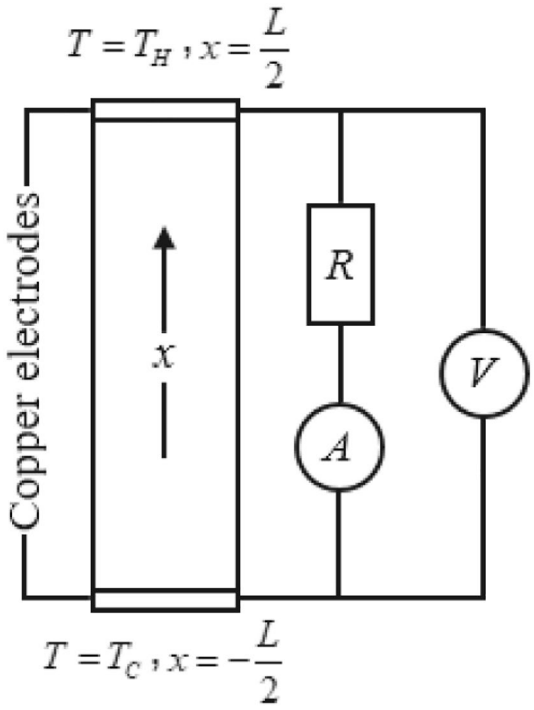

Fig. 1. A FGTED with cold side temperature (T_C) at location $x = -\frac{L}{2}$ and hot side temperature (T_H) at location $x = \frac{L}{2}$. The external circuit consists of an ammeter (A), an external load (R), and a voltmeter (V).

Using Eq. (1), E can be defined as,

$$E=\rho \mathrm{J}+\mathrm{S}\frac{\mathrm{dT}}{\mathrm{dx}}. \tag{7}$$

Substituting Eq. (7) into Eq. (3),

$$\frac{\mathrm{dq}}{\mathrm{dx}}=\rho \mathrm{J}^2+\mathrm{SJ}\frac{\mathrm{dT}}{\mathrm{dx}}. \tag{8}$$

Further, differentiating Eq. (2) with respect to x and substituting Eq. (8) into it, the temperature distribution governing equation obtained is given as,

$$\kappa\frac{\mathrm{d}^2\mathrm{T}}{\mathrm{dx}^2}+\frac{\mathrm{d}\kappa}{\mathrm{dx}}\frac{\mathrm{dT}}{\mathrm{dx}}-J\frac{\mathrm{dS}}{\mathrm{dx}}T=-\rho \mathrm{J}^2, \tag{9}$$

where, J is an unknown constant. Eq. (9) needs to be solved mathematically for obtaining the temperature distribution along the length of the FGTED.

For obtaining the solution to Eq. (9), the FDM is used for transforming the differential equations into a system of algebraic equations[48,49]. The FGTED is discretized into n intervals with Δx being the interval size, given as,

$$x_i=\mathrm{i}\Delta \mathrm{x}, \tag{10a}$$

$$\Delta x=\frac{\mathrm{L}}{\mathrm{n}}, \tag{10b}$$

where, i = 0, 1, 2, …, n, and L is the total length of the FGTED. The parameters (T, S, κ, and ρ) at different locations (x_i) are denoted as T_i, S_i, κ_i, and ρ_i.

Using the derivative approximations incorporating central differences, the derivative terms of Eq. (9) can be expressed as,

$$\frac{\mathrm{d}^2\mathrm{T}}{\mathrm{dx}^2}\approx\frac{\mathrm{T_{i+1}}-2\mathrm{T_i}+\mathrm{T_{i-1}}}{\Delta \mathrm{x}^2}, \tag{11a}$$

$$\frac{\mathrm{d}\kappa}{\mathrm{dx}}\frac{\mathrm{dT}}{\mathrm{dx}}\approx\frac{(\kappa_{i+1}-\kappa_{i-1})(T_{i+1}-T_{i-1})}{4\Delta \mathrm{x}^2}, \tag{11b}$$

$$\frac{\mathrm{dS}}{\mathrm{dx}} \approx \frac{S_{\mathrm{i+1}} - S_{\mathrm{i-1}}}{2\Delta \mathrm{x}}. \tag{11c}$$

On substituting Eq. (11) into Eq. (9), the temperature distribution governing equation modifies to,

$$\kappa_{\mathrm{i}} \frac{T_{\mathrm{i+1}} - 2\mathrm{T_i} + \mathrm{T_{i-1}}}{\Delta x^2} + \kappa_{\mathrm{i+1}} \frac{(\kappa_{\mathrm{i+1}} - \kappa_{\mathrm{i-1}})(T_{\mathrm{i+1}} - T_{\mathrm{i-1}})}{4\Delta \mathrm{x}^2} - J \frac{S_{\mathrm{i+1}} - S_{\mathrm{i-1}}}{2\Delta \mathrm{x}} T_{\mathrm{i}} = -\rho_{\mathrm{i}} J^2, \tag{12}$$

where, i = 1, 2, 3, …, n-1. At i = 0 and i = n, the limiting conditions are used as given by Eq. (6). Eq. (12) can be simplified as,

$$(\alpha - \beta)\mathrm{T_{i-1}} + (-2\alpha - \gamma)\mathrm{T_i} + (\alpha + \beta)\mathrm{T_{i+1}} = -\rho_{\mathrm{i}} \mathrm{J}^2, \tag{13}$$

where, $\alpha = \frac{\kappa_{\mathrm{i}}}{\Delta x^2}, \beta = \kappa_{\mathrm{i+1}} \frac{(\kappa_{\mathrm{i+1}} - \kappa_{\mathrm{i-1}})}{4\Delta \mathrm{x}^2}$, and $\gamma = J \frac{S_{\mathrm{i+1}} - S_{\mathrm{i-1}}}{2\Delta \mathrm{x}}$.

Using Eqs. (10a), (10b), (13) and solving for x = 1 to n-1, a (n-2) x (n-2) tridiagonal matrix is obtained given as,

$$\begin{pmatrix} d_1 & e_1 & 0 & 0 & 0 & 0 \\ c_2 & d_2 & e_2 & 0 & 0 & 0 \\ 0 & c_3 & d_3 & e_3 & 0 & 0 \\ 0 & 0 & c_4 & d_4 & e_4 & 0 \\ & & & & \ddots & \vdots \\ 0 & 0 & 0 & c_5 & & \\ 0 & 0 & 0 & 0 & \dots & d_{n-1} \end{pmatrix} \begin{pmatrix} T_1 \\ T_2 \\ T_3 \\ T_4 \\ \vdots \\ T_{n-1} \end{pmatrix} = \begin{pmatrix} b_1 \\ b_2 \\ b_3 \\ b_4 \\ \vdots \\ b_{n-1} \end{pmatrix}. \tag{14}$$

Eq. (14) can be denoted as,

$$[C]\{T_{\mathrm{i}}\} = \{b_{\mathrm{i}}\}, \tag{15}$$

where, [C] is the coefficient matrix, $\{T_i\}$ is unknown temperature vector at discrete points i = 1, 2, …, n-1 and $\{b_i\} = -\rho_i J^2$.

The elements of the matrix [C] are computed using the Thomas algorithm, a fast and direct (non-iterative) method specifically tailored for solving tridiagonal systems of linear equations[50,51]. By applying the finite difference method in conjunction with the Thomas algorithm to Eq. (9), the absolute temperature distribution $T(x)$ is obtained, accounting for the spatially varying thermoelectric properties in the FGTED.

Validation study

To validate the accuracy and efficacy of the developed solution, the temperature distributions obtained using the present solution method are compared with that given by Jin et al.[19] The authors considered exponential distribution of the thermoelectric properties given as,

$$\kappa = \kappa_{\mathrm{C}} \exp\left(\frac{\beta \mathrm{x}}{\mathrm{L}}\right), \tag{16a}$$

$$S = \mathrm{S_C} \exp\left(\frac{\beta \mathrm{x}}{\mathrm{L}}\right), \tag{16b}$$

$$\rho = \rho_{\mathrm{C}} \exp\left(\frac{\gamma \mathrm{x}}{\mathrm{L}}\right), \tag{16c}$$

where, κ_C = 1.35 W/m/K, S_C = 180 μV/K, ρ_C = 0.7 x 10^{-5} Ω-m, T_H = 600 K, T_C = 300 K, and L = 5 mm. For different values of the property variation parameters (β, γ) and current density (J), the temperature distributions obtained using the present solution method matches well with the published results as presented in Fig. 2.

Modelling of the FGTED

In this section, a FGTED model is developed to study the effect of grain size gradation on the power output. Smaller and larger grains are heterogeneously distributed along the length, with each location exhibiting distinct volume fractions. The variation in the volume fractions along the length of the FGTED is defined using a power's law function given as[52],

$$V_S = 1 - \left(\frac{1}{2} + \frac{\mathrm{x}}{\mathrm{L}}\right)^{\mathrm{n}}, \tag{17a}$$

$$V_S + V_L = 1, \tag{17b}$$

where, V denotes the volume fraction of the grains, x is the position at which the volume fraction is evaluated, L is the total length varying from $x = -\frac{L}{2}$ to $x = \frac{L}{2}$, and n is the volume fraction variation parameter. For n = 0 and n = ∞, the FGTED gets converted to homogeneous thermoelectric device composed entirely of larger or smaller grains, respectively. From here on, the subscripts '$_S$' and '$_L$' refers to the smaller and larger sizes of the ZnO grains, respectively.

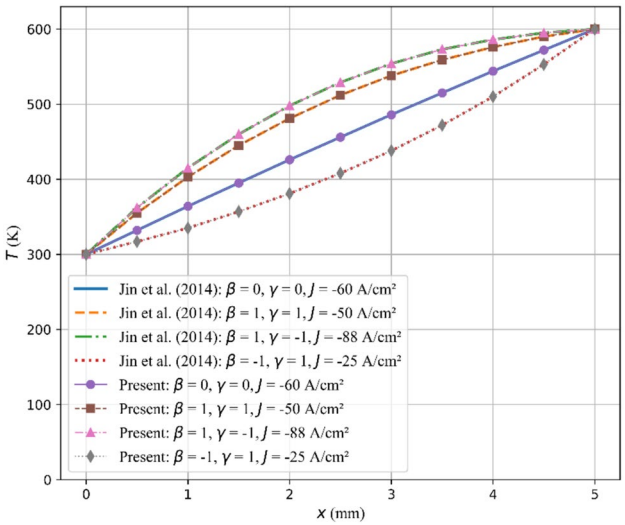

Fig. 2. Comparison of T vs. x curves obtained using the present solution method with the known solution.

After determining the volume fractions (V_S, V_L) of the grains at different locations (x), it is essential to assume temperature at the locations as the ZnO grains of different sizes exhibit different thermoelectric properties because of the temperature dependency. Therefore, a linear distribution of temperature is considered along the length of the FGTED given as[20],

$$T = T_C + (T_H - T_C)\left(\frac{1}{2} + \frac{x}{L}\right), \tag{18}$$

where, T_C and T_H are the cold and the hot side temperatures at locations $x = -\frac{L}{2}$ and $x = \frac{L}{2}$, respectively.

Thereafter, the effective temperature dependent thermoelectric properties ($S_{eff.}$, $\kappa_{eff.}$, and $\rho_{eff.}$), accounting for the volumetric ratios of smaller and larger ZnO grains, at locations (x) are given by[20],

$$S_{eff.} = \mathrm{S_S V_S + S_L V_L}, \tag{19a}$$

$$\kappa_{eff.} = \kappa_S \left[1 + \frac{3\mathrm{V_L}\,(\kappa_L - \kappa_S)}{\mathrm{V_S}\,(\kappa_L - \kappa_S) + 3\kappa_S}\right], \tag{19b}$$

$$\rho_{eff.} = \rho_S \left[1 + \frac{3\mathrm{V_L}\,(\rho_L - \rho_S)}{\mathrm{V_S}\,(\rho_L - \rho_S) + 3\rho_S}\right]. \tag{19c}$$

Further, the COMSOL Multiphysics (version 5.5) is used for determining the power output of the FGTED model using the obtained effective thermoelectric properties. The thermoelectric module is used in conjugation with the electric circuit module. The solver is configured to a fully coupled, direct, and stationary study. The developed computational model of the FGTED is presented in Fig. 3. A voltmeter, an ammeter, and an external load of 1 Ω is connected to the FGTED (as represented in the external circuit diagram given in Fig. 1). The material properties for ZnO and the copper electrodes are listed in Table 1.

Validation study

To evaluate the efficacy and accuracy of the developed computational model, it is configured with the material and the temperature dependent properties of a homogeneous $(Bi_{0.5}Sb_{0.5})_2Te_3$ thermoelectric device, as given in Table 2 and Table 3, respectively. It is then simulated and the obtained voltage and current outputs are compared with the known results[54]. To ensure consistency, the dimensions (1 mm x 1 mm x 5.8 mm), the cold side temperature (273 K), and the hot side temperature (373 K) are adopted from the reference study.

In Eq. (17a), setting $n = 0$ converts the FGTED into a homogeneous thermoelectric device consisting of a uniform grain size or single material. This eliminates the need for calculation of the effective thermoelectric properties. Therefore, the $S_{eff.}$, $\kappa_{eff.}$, and $\rho_{eff.}$ are directly replaced by the S, κ, and ρ values of Table 3. The voltage and the current output comparison with the known results is shown in Fig. 4. It can be observed from Fig. 4 that the present results match well with the known results.

Temperature dependent thermoelectric properties

In this section, the temperature dependent thermoelectric properties for ZnO grains of sizes 3.51 ± 0.18 μm and 5.75 ± 0.06 μm are reported in the temperature range 120 K to 345 K. The co-precipitation, spark plasma sintering (SPS), and heat treatment techniques are employed for preparation of two different samples; (i) AZO-S, consisting of 3.51 ± 0.18 μm sized ZnO grains, and (ii) AZO-H, consisting of 5.75 ± 0.06 μm sized ZnO grains.

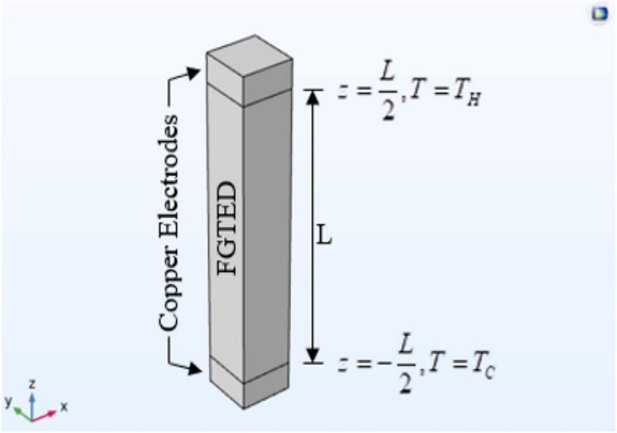

Fig. 3. Developed computational model of the FGTED of length *L*. The lateral dimensions are taken as 2 mm x 2 mm. The dimensions of copper electrode are 2 mm x 2 mm x 1 mm.

Properties	ZnO	Copper electrode
Density (Kg/m^3)	5610	8700
Heat capacity (J/Kg/K)	494	385
Relative permittivity	1	1
Electrical resistivity (Ω-m)	Temperature dependent	1.6672×10^{-8}
Thermal conductivity (W/m/K)	Temperature dependent	400

Table 1. Material properties for ZnO and copper electrodes[53,54].

Description	Values
Density (Kg/m^3)	7740
Heat capacity (J/Kg/K)	154.4
Relative permittivity	1

Table 2. $(Bi_{0.5}Sb_{0.5})_2Te_3$ material properties[54].

T (K)	*S* (μV/K)	*κ* (W/m/K)	*ρ* (Ω-m)
100	75	2.5	0.5405×10^{-05}
150	125	2	0.7042×10^{-05}
200	170	1.55	1×10^{-05}
250	200	1.35	1.3888×10^{-05}
300	218	1.28	1.6666×10^{-05}
350	225	1.35	1.8181×10^{-05}
400	218	1.75	1.4285×10^{-05}

Table 3. $(Bi_{0.5}Sb_{0.5})_2Te_3$ temperature dependent thermoelectric properties[54].

Additionally, a mathematical model is also developed using which the properties can be determined at any temperature point in the specified temperature range.

Experimental procedure

The Al-doped ZnO powder is synthesized via co-precipitation method, as described in detail in our previous work[55]. The synthesized powder is then sintered employing the SPS technique (Dr. Sinter SPS-625, Fuji Electronic Industrial Co. Ltd., Japan). For preparing the dense Al-doped ZnO samples, a targeted amount of synthesized powder is loaded into a 10.5 mm graphite die. To prevent direct contact between the powder and the die walls or

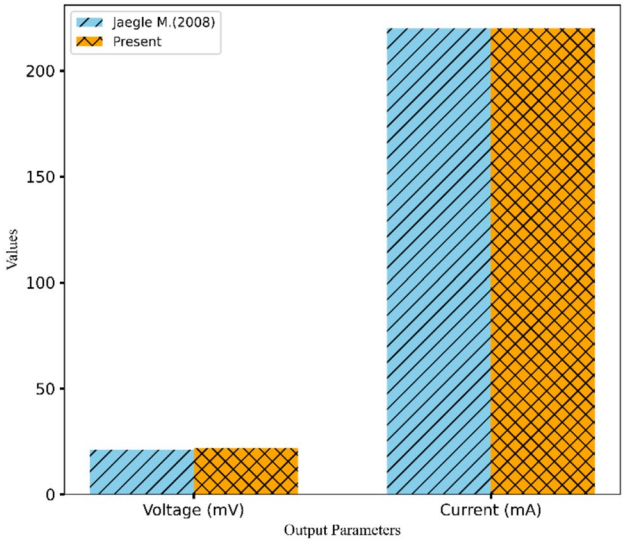

Fig. 4. Comparison of the present results with the known results of Jaegle M[54].

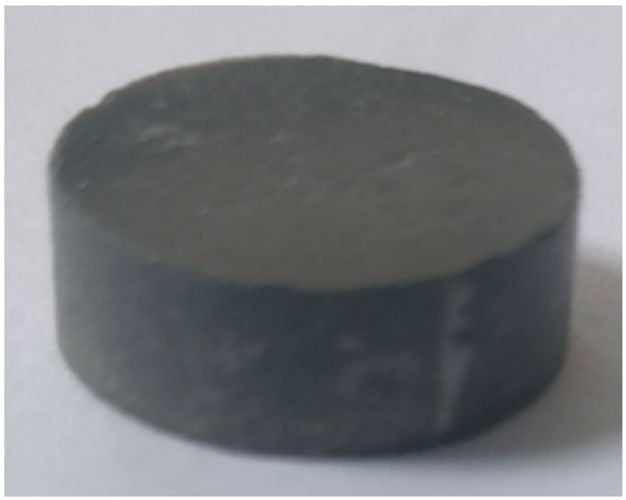

Fig. 5. Experimentally fabricated ZnO thermoelectric device sample (AZO-S).

punches during the sintering process, a 0.25 mm thick graphite sheet lining is used. An initial uniaxial pressure of 20 MPa is applied to the powder to form a green compact. The compact is then subjected to SPS in Argon atmosphere, with a rapid heating rate of 100 °C/min until a sintering temperature of 1000 °C is reached, under a constant pressure of 50 MPa and a holding time of 5 minutes at the peak temperature.

After the sintering process, the pellets/samples are allowed to cool within the SPS chamber. Thereafter, the pellets/samples are carefully removed and the surfaces are cleansed using sandpaper to eliminate any residual graphite foil. To obtain enhanced grain size, one of the sintered samples is subjected to a secondary annealing process in a tubular furnace. It is heated at a slower rate of 5 °C/min and is held at 1000 °C peak temperature for 10 hours in Argon atmosphere, followed by natural cooling within the furnace. The slow heating rate facilitates gradual atomic diffusion and ensures uniform densification with controlled grain growth. Also, the extended holding time provides sufficient time for grain boundary migration and more uniform grain growth. The pellet/sample without post-processing is referred to as AZO-S, while the annealed sample is denoted as AZO-H. The densities of AZO-S and AZO-H are found to be 97.8% and 98.2%, respectively. Both the samples possess a uniform thickness of 3 mm. The fabricated AZO-S sample is shown in Fig. 5.

Further, to investigate the structural and physical characteristics of the prepared samples, a series of characterization techniques are employed. The crystalline structure and phase composition of the sintered pellets/samples are analysed using an X-ray diffractometer (Anton-Paar XRDynamics-500) equipped with Cu-Kα radiation ($\lambda = 0.15406$ nm). The measurements are conducted over a 2θ range of 20° to 70°, using a step size of 0.02° and a scan rate of 2 seconds per step. The microstructural features, such as morphology and grain size, are examined using FESEM (Sigma-300 Carl Zeiss). Additionally, the thermoelectric properties as well as

the resulting figure of merit, are measured using a physical property measurement system (DynaCool PPMS, Quantum Design).

Microstructural analysis results

The crystallographic phase and the microstructural characterization of AZO-S and AZO-L samples are analysed using X-ray diffraction (XRD) as illustrated in Fig. 6. It can be observed from Fig. 6 that the diffraction peaks 100, 002, 101, 102, 110, 103, 200, 112, 201 occur at 2θ values 31.74°, 34.37°, 36.23°, 47.50°, 56.58°, 62.83°, 66.35°, 67.97°, and 69.07°, respectively. This indicates the standard ZnO wurtzite structure. The peaks match with the reference pattern as in the JCPDS card no. #36-1451. The observed reflections through the Xpert high score are similar to a hexagonal wurtzite structure of ZnO which corresponds to a space group of P63mc. Also, the multiple peaks detected in the XRD analysis confirms the polycrystalline nature of the material. The sharp and intense diffraction peaks indicate that ZnO exhibits high crystallinity. The results confirm the retention of a single-phase ZnO structure in both the conditions, with no evidence of secondary phases.

Additionally, the average crystallite size of the pellets/samples are calculated before and after the annealing process using the Debye-Scherer formula, given as,

$$D = \frac{k\lambda}{\beta \cos\theta}, \tag{20}$$

where, D represents the crystalline size, k corresponds to the shape factor with value 0.94, λ indicates the wavelength of the incident X-ray, β represents the full-width half maximum (FWHM) of the peaks in radian, and θ is the Bragg's angle in degree.

The crystalline size of AZO-S and AZO-H are measured to be 44.11 nm and 54.44 nm, respectively. This indicates that the post-sintering heat treatment led to an enhancement in the crystalline size. The dislocation density (δ), given as[56],

$$\delta = \frac{1}{D^2}, \tag{21}$$

decreased from 0.51 x 10^{-3} nm^{-2} for AZO-S to 0.34 x 10^{-3} nm^{-2} for AZO-H, indicating reduced lattice imperfections due to improved crystallinity and grain growth after heat treatment.

Surface morphology analysis

For performing the microstructure analysis, the surfaces of the bulk sintered pellets/samples are meticulously polished using a diamond paste, followed by colloidal silica, to achieve a smooth and defect-free finish. The Field Emission Scanning Electron Microscopy (FESEM) is then performed. Scaled micrographs are acquired from multiple representative regions of the sample and grain sizes for approximately ~150 individual grains are quantified using the linear intercept method. The SEM micrographs of AZO-H reveal notable microstructural changes, induced due to post-sintering heat treatment, when compared with the AZO-S sample. It can be observed from Fig. 7(a) that the AZO-S sample exhibits a fine-grained microstructure with an average grain size of 3.51 ± 0.18 μm. In contrast, Fig. 7(b) shows noticeable grain coarsening, leading to an increased average grain size of 5.75 ± 0.06 μm in the AZO-H sample. Since the sintering temperature employed (1000 °C) is significantly below the melting point of ZnO (~1975 °C), the grain growth can be attributed to solid-state diffusion and

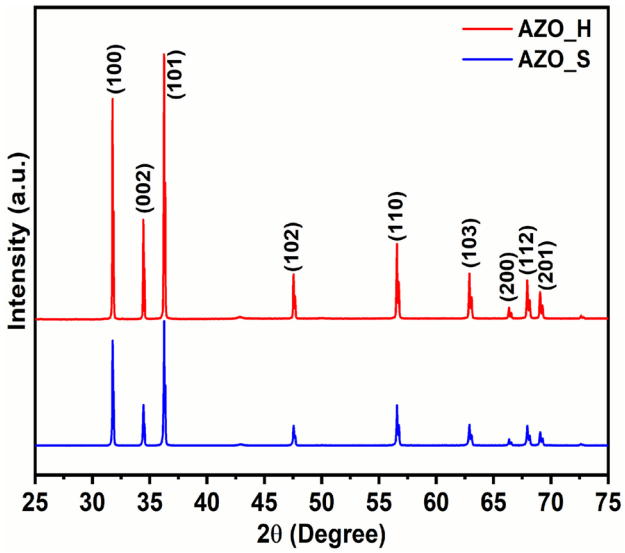

Fig. 6. XRD diffraction pattern for sintered Al-doped ZnO samples AZO-S and AZO-H.

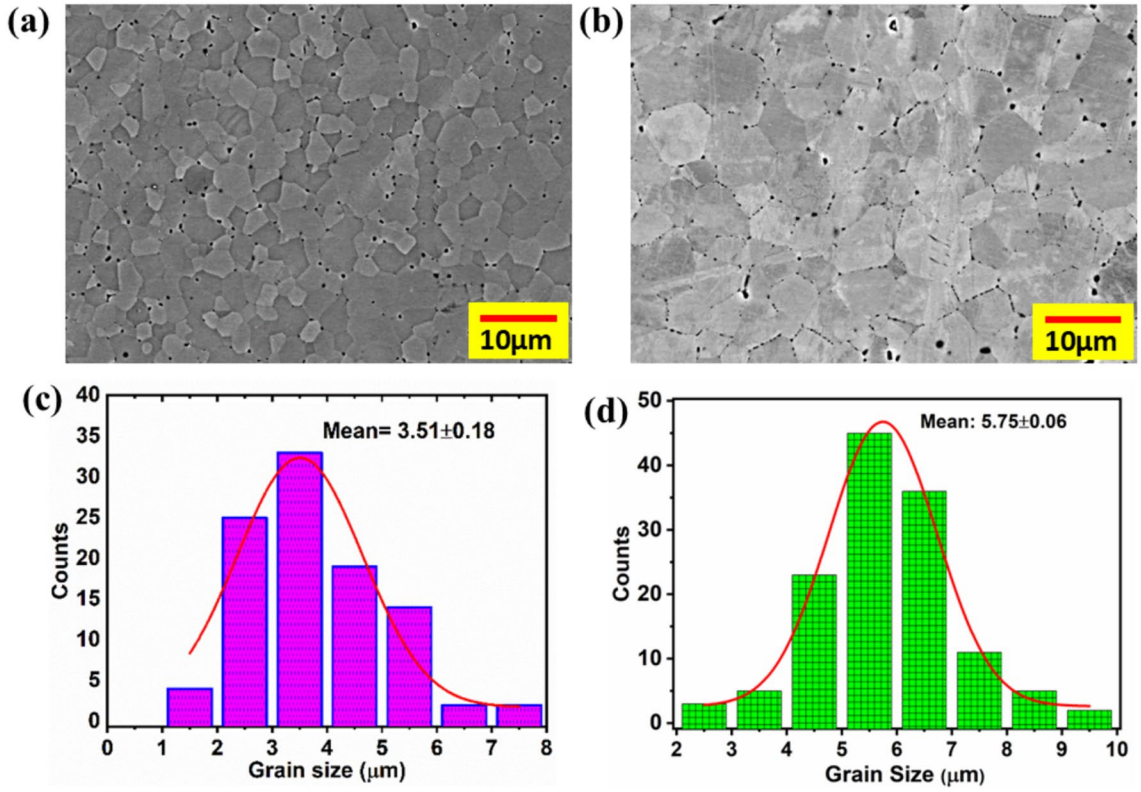

Fig. 7. SEM images of fabricated samples; (**a**)AZO-S, (**b**)AZO-H. Grain size distribution hysterogram; (**c**) AZO-S, (**d**) AZO-H.

Ostwald ripening mechanisms, which drive grain boundary migration and coalescence without melting, rather than to any liquid phase processes[57].

The grain size distribution hysterogram is also given in Fig. 7(c) and Fig. 7(d) for AZO-S and AZO-H samples, respectively. Fig. 7(c) and Fig. 7(d) further confirms the mean grain size of ZnO present in the fabricated samples. This observed grain growth suggests an enhanced grain boundary mobility and a substantial microstructural evolution due to the thermal activation during the post-sintering heat treatment. Small number of pores can also be observed in both the samples, predominantly at the grain boundaries. These pores can potentially reduce both the electrical and the thermal conductivity of the samples.

Thermoelectric properties measurements

To measure the thermoelectric properties, both AZO-S and AZO-H pellets/samples are cut into rectangular bars of dimensions 2 mm x 2 mm x 10 mm using a diamond saw. Four-probe electrical contacts are prepared on the bar shaped samples, using silver paste and epoxy, to ensure reliable electrical measurements. Thereafter, the thermoelectric properties (S, κ, ρ) and the figure of merit (ZT) are evaluated using a Physical Property Measurement System (PPMS) in the temperature range of 120 K to 345 K.

The κ vs. T curve for the fabricated samples are given in Fig. 8(a). It can be observed from Fig. 8(a) that the κ for AZO-S is 9.19 W/m/K at 120 K and remains nearly constant throughout the measured temperature range. For AZO-H, the κ is 85 W/m/K at 120 K and progressively decreases with increasing temperature, reaching 44.70 W/m/K at 345 K. This behaviour is typical in large-grained polycrystalline ceramics and is primarily due to increased phonon-phonon scattering at higher temperatures[58]. Meanwhile, the AZO-H sample is exhibiting higher κ in the entire temperature range of 120 K to 345 K. This is mainly due to the larger grain size resulting to reduced phonon scattering.

The S vs. T curves for the AZO-S and AZO-H samples are presented in Fig. 8(b). The curves confirm the *n-type* conduction behaviour in both the fabricated samples, with values S = -63 µV/K for AZO-S and S = -106 µV/K for AZO-H at 345 K. The ρ vs. T curves are given in Fig. 8(c). It can be observed from Fig. 8(c) that the AZO-H exhibits lower ρ in the entire temperature range. The ρ for AZO-H is 1.18 x 10^{-4} Ω-m and for AZO-S is 5.98 x 10^{-4} Ω-m at 345 K and remains nearly constant throughout the temperature range. This observation is attributed to the grain boundary scattering effect. The presence of larger grains in the AZO-H sample reduces the number of grain boundaries, thereby minimizing carrier scattering and lowering resistivity. Further, the ZT vs. T curve for the samples are given in Fig. 8(d). It can be observed from Fig. 8(c) that despite of the higher κ exhibited by the AZO-H sample in the entire temperature range, it demonstrates an enhanced ZT. The maximum ZT value of 0.00073 is observed for AZO-H at 345 K. For AZO-S, the maximum ZT value of 0.00026

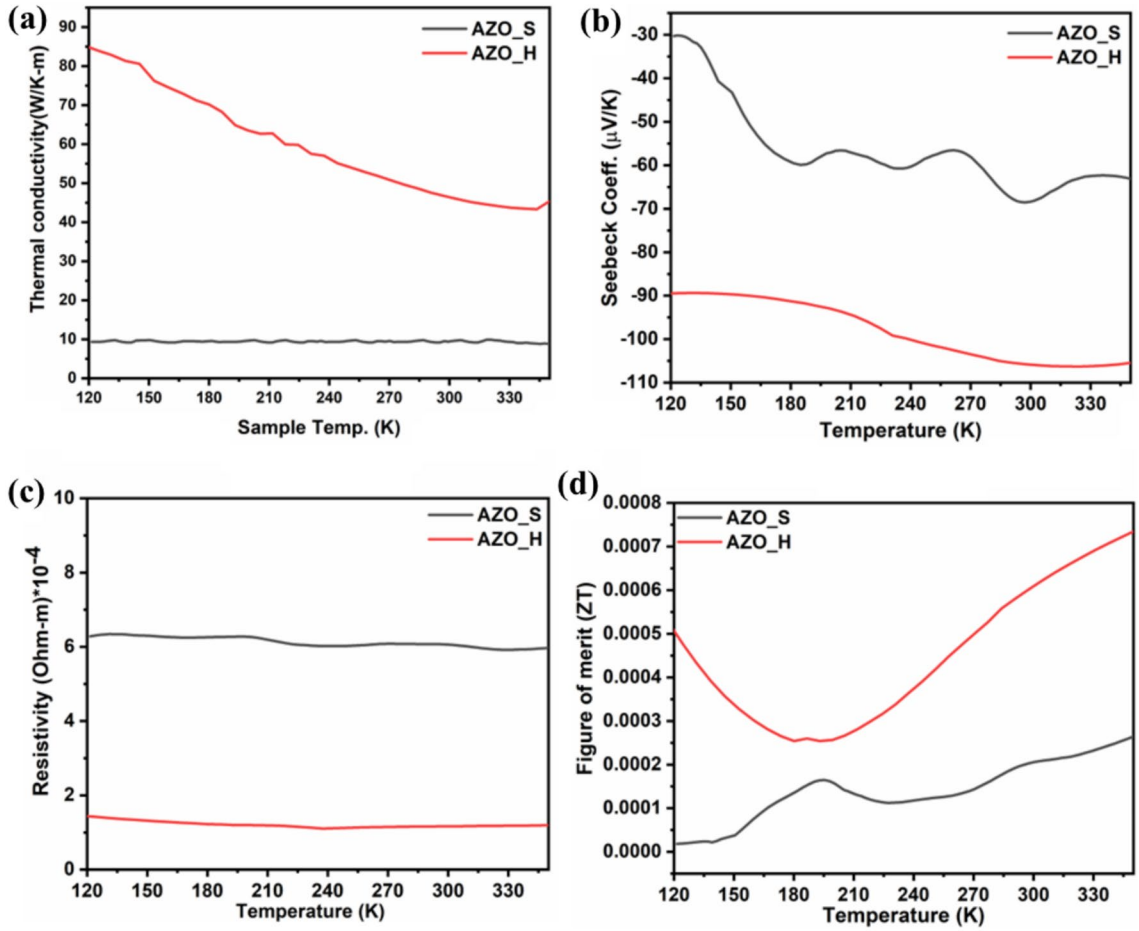

Fig. 8. Temperature dependent properties; (**a**) κ, (**b**) S, (**c**) ρ, (**d**) ZT.

occurs at the same temperature. This represents a 65 % improvement in the thermoelectric performance for the large-grain sized sample (AZO-H).

Development of thermoelectric properties prediction model

The thermoelectric properties in the temperature range 120 K to 345 K exhibit non-linear relationship with temperature (can be observed in Fig. 8). Therefore, third-degree polynomial equations are employed to model the behaviour, given as,

$$S = S_0\left[1+\alpha_1\left(\frac{T-T_0}{T_0}\right)+\alpha_2\left(\frac{T-T_0}{T_0}\right)^2+\alpha_3\left(\frac{T-T_0}{T_0}\right)^3\right], \tag{22a}$$

$$\kappa=\kappa_0\left[1+\beta_1\left(\frac{T-T_0}{T_0}\right)+\beta_2\left(\frac{T-T_0}{T_0}\right)^2+\beta_3\left(\frac{T-T_0}{T_0}\right)^3\right], \tag{22b}$$

$$\rho=\rho_0\left[1+\gamma_1\left(\frac{T-T_0}{T_0}\right)+\gamma_2\left(\frac{T-T_0}{T_0}\right)^2+\gamma_3\left(\frac{T-T_0}{T_0}\right)^3\right], \tag{22c}$$

where, the subscript '$_0$' represents the properties at cold side temperature T_0. The curve-fitting method is used to determine values of the coefficients α, β, and γ. Eqs. 22 (a-c) allows determining the thermoelectric properties (S, κ, ρ) at any temperature point (T) in the specified temperature range for 3.51 ± 0.18 μm and 5.75 ± 0.06 μm sized ZnO grains.

For 3.51 ± 0.18 μm ZnO grains;

S_0 = -31.3333 μV/K, α_1 = 1.8385, α_2 = -1.1197, α_3 = 0.2295, κ_0 = 9.6303 W/m/K, β_1 = -0.1758, β_2 = 0.2562, β_3 = -0.0984, ρ_0 = 0.0006307 Ω-m, γ_1 = -0.0256, γ_2 = -0.0043, γ_3 = 0.0018, T_0 = 120 K.

For 5.75 ± 0.06 μm ZnO grains;

S_0 = -88.6666 μV/K, α_1 = -0.0236, α_2 = 0.2190, α_3 = -0.0792, κ_0 = 84.3774 W/m/K, β_1 = -0.3279, β_2 = -0.0624, β_3 = 0.0535, ρ_0 = 0.0001512 Ω-m, γ_1 = -0.1623, γ_2 = -0.1843, γ_3 = 0.1159, T_0 = 120 K.

Performance analysis

In this section, the power output, figure of merit, and power factor for the FGTED composed of ZnO grains of sizes 3.51 ± 0.18 μm (smaller) and 5.75 ± 0.06 (larger) are determined and put to a comparative analysis. The value of the volume fraction variation parameter (n) is varied from 0 to ∞. The temperature dependent thermoelectric properties for the FGTED with values of n in the range 0 to ∞, calculated using Eqs. (19a), (19b), and (19c), are represented in Fig. 9.

It can be observed from Fig. 9 that the S, κ, and ρ for $n = 0.5$, in the specified tempearture range, lie in between those for $n = 0$ (homogeneous thermoelectric device composed entirely of 5.75 ± 0.06 μm sized ZnO grains) and $n = \infty$ (homogeneous thermoelectric device composed entirely of 3.51 ± 0.18 μm sized ZnO grains). The κ of the FGTED with $n = 0$ is greater than that exhibited by the device when $n = 0.5$ and $n = \infty$. This might be due to the reduced phonon scattering at the grain boundaries causing incresement in the lattice component of κ.

Power output

To determine the grain volume fraction distribution that yields the maximum power output, the volume fraction variation parameter (n) is varied from 0 to ∞, and the corresponding power outputs are evaluated and compared. Fig. 10 represents the power output of the FGTED for different values of n. The FGTED is assumed to have a length of 10 mm and lateral dimensions of 2 mm x 2 mm.

It can be observed from Fig. 10 that the power output is minimum for $n = \infty$ (homogeneous thermoelectric device composed entirely of 3.51 ± 0.18 μm sized ZnO grains). This primarily may be due to the higher electrical resistivity exhibited by the smaller ZnO grains. Further, as the volume fraction of the large ZnO grains is

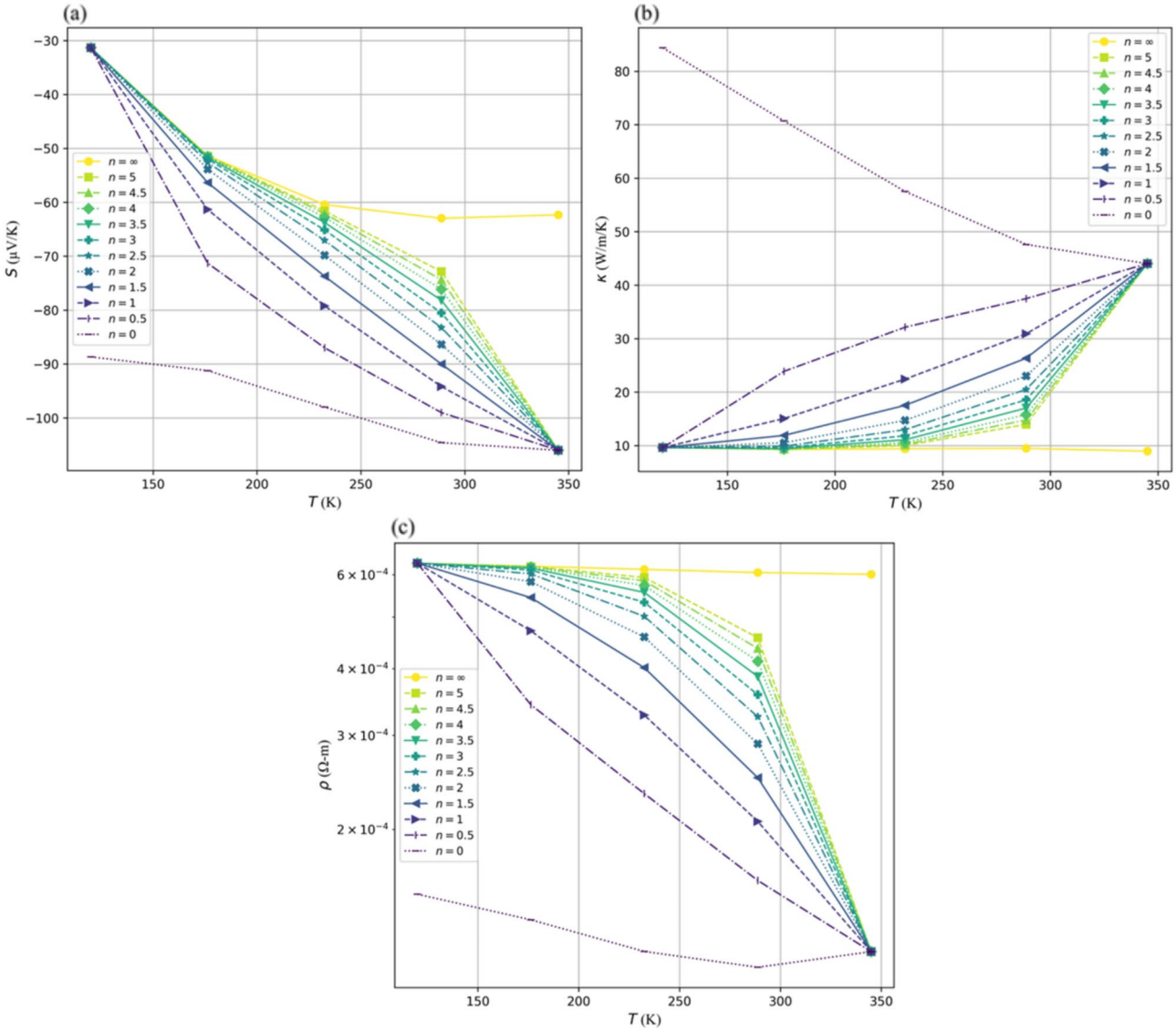

Fig. 9. Thermoelectric properties in the temperature range 120 K - 345 K for the FGTED composed of 3.51 ± 0.18 μm and 5.75 ± 0.06 μm grain sizes of ZnO; (**a**) S, (**b**) κ, (**c**) ρ.

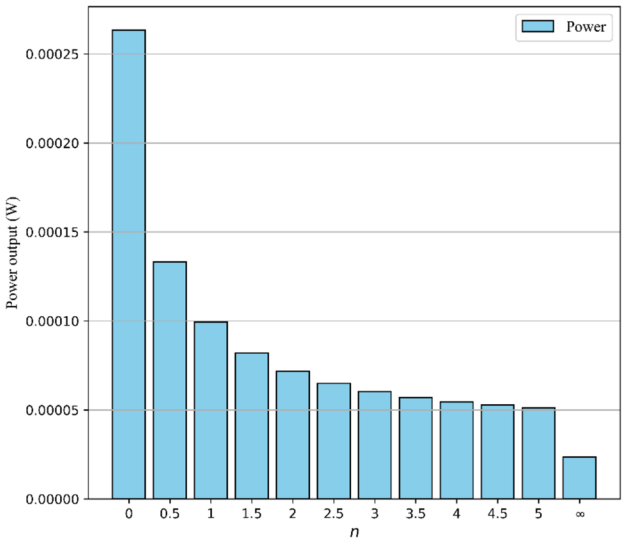

Fig. 10. Power output vs. n for the FGTED composed of 3.51 ± 0.18 μm and 5.75 ± 0.06 μm μm sized ZnO grains. The cold and the hot side temperatures across the FGTED are 120 K and 345 K, respectively.

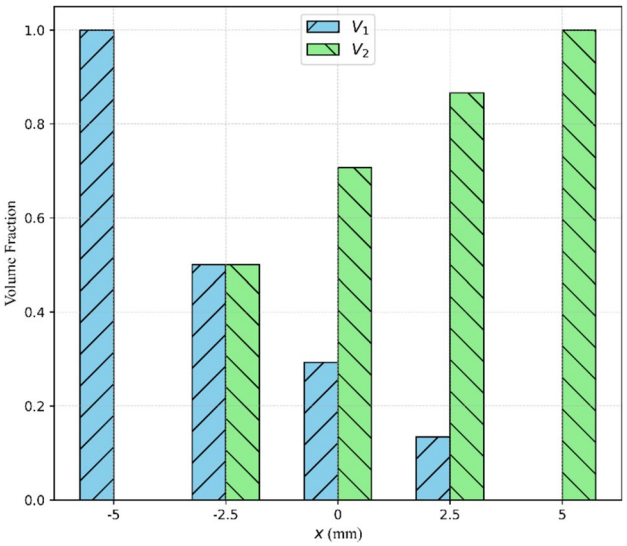

Fig. 11. Volume fraction distribution of smaller (3.51 ± 0.18 μm) and larger (5.75 ± 0.06 μm) sized ZnO grains at different locations along the length of the FGTED when n = 0.5.

increasing (value of n decresing from ∞ to 0), the power output is increasing. The magnitude of power output when n = ∞ is 2.36 x 10^{-5} W, whereas for n = 0.5, it is 1.33 x 10^{-4} W. This represents an order of magnitude increase, highlighting the potential of functional grain size graded devices. Inspite of the enhanced κ (Fig. 9(b)), the maximum power output is obtained for the FGTED with n = 0. This is mainly because of the enhanced S and reduced ρ in the entire temperature range.

The volume fraction distribution of smaller and larger grains when n = 0.5 is shown in Fig. 11 which elucidates the dominance of large ZnO grains. However, the maximum power output of 2.63 x 10^{-4} W is obtained for n = 0 (homogeneous device composed entirely of 5.75 ± 0.06 μm sized ZnO grains), which is greater than the power output of FGTED with n = 0.5 by 97.74 %.

Figure of merit and power factor

For assessing the performance of TEMs/TEDs, the figure of merit (ZT) serves as a key parameter. It is a dimensionless quantity given as[11,12],

$$ZT = \frac{S^2 T}{\kappa \rho}, \tag{23}$$

where S, κ, ρ, and T are the seebeck coefficient, thermal conductivity, electrical resistivity, and absolute temperature, respectively. In contrast, the power factor (PF) of a TED quantifies the ability of converting heat into electrical energy. The thermal conductivity is not included, as its primary function is to sustain the temperature difference across the ends of the TED. The PF is given as[59],

$$PF = \frac{S^2 T}{\rho}. \tag{24}$$

The zT vs. T and the PF vs. T curves for the FGTED when n = 0, 0.5, and ∞ are presented in Fig. 12(a) and Fig. 12(b), respectively. It can be observed from Fig. 12(a) that the ZT values for n = 0 is consistently higher when compared with the ZT values for n = 0.5 and n = ∞ in the entire temperature range. A similar trend for the PF can also be observed from Fig. 12(b). This supports the conclusion that the maximum power output is obtained for the FGTED with n = 0.

Temperature distribution

To ensure that the linear temperature distribution assumption closely aligns with the temperature distribution derived using Eq. (9), a comparison study is performed. For the FGTED with n = 0, 0.5, and ∞, the effective thermoelectric properties at different locations obtained using Eqs. (19a), (19b), and (19c) are curve fitted to power's law spatial distribution equations given as[52],

$$S(x) = S_0 + (S_L - S_0)\left(\frac{1}{2} + \frac{x}{L}\right)^p, \tag{25a}$$

$$\kappa(x) = \kappa_0 + (\kappa_L - \kappa_0)\left(\frac{1}{2} + \frac{x}{L}\right)^q, \tag{25b}$$

$$\rho = \rho_0 + (\rho_L - \rho_0)\left(\frac{1}{2} + \frac{x}{L}\right)^w, \tag{25c}$$

where, $S(x)$, $\kappa(x)$, and $\rho(x)$ are the Seebeck coefficient, thermal conductivity, and electrical resistivity at positions (x). p, q, and w are the property variation parameters. The subscripts '$_0$' and '$_L$' correspond to the properties at x = -5 mm and x = 5mm, respectively. L = 10 mm is the total length of the FGTED.

For the FGTED with n = 0,

S_0 = -88.6666 μV/K, κ_0 = 84.3774 W/m/K, ρ_0 = 0.0001512 Ω-m, S_L = -106 μV/K, κ_L = 44.0272 W/m/K, ρ_L = 0.000118 Ω-m, p = 0.9589, q = 0.6602, w = 0.2864.

For the FGTED with n = 0.5,

S_0 = -31.3333 μV/K, κ_0 = 9.6303 W/m/K, ρ_0 = 0.0006307 Ω-m, S_L = -106 μV/K, κ_L = 44.0272 W/m/K, ρ_L = 0.000118 Ω-m, p = 0.4350, q = 0.6368, w = 0.3939.

For the FGTED with n = ∞,

S_0 = -31.3333 μV/K, κ_0 = 9.6303 W/m/K, ρ_0 = 0.0006307 Ω-m, S_L = -62.3333 μV/K, κ_L = 8.9688 W/m/K, ρ_L = 0.0006012 Ω-m, p = 0.2352, q = 2.8930, w = 0.8434.

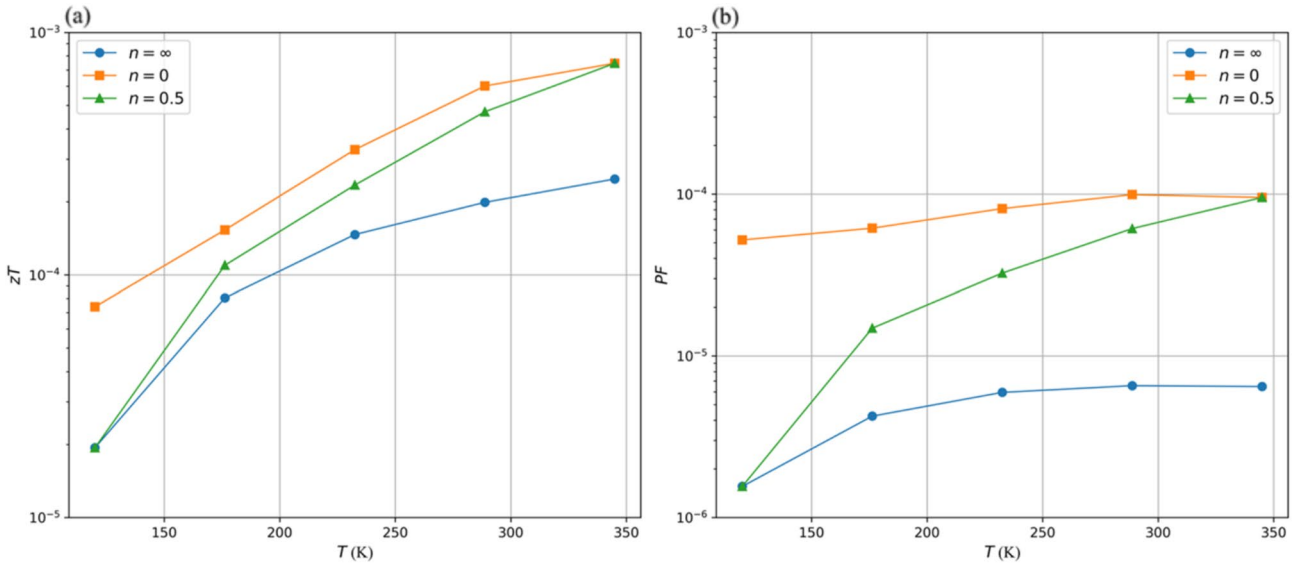

Fig. 12. Thermoelectric performance of the FGTED composed of 3.51 ± 0.18 μm and 5.75 ± 0.06 μm grain sizes of ZnO; (**a**) ZT vs. T curves, (**b**) PF vs. T curves.

Figure 13 represents the comparison of the temperature distributions, obtained using Eq. (9) with the linear, for the FGTED. It can be observed from Fig. 13 that the resulting temperature distributions closely approximates a linear pattern. This justifies the assumption of the linear temperature distribution in the present study.

Case study

To study the effect of grain size in the higher temperature range (375 K - 675K), a S-FGTED composed of ZnO grains of sizes 0.18 ± 0.03 μm (smaller) and 1.2 ± 0.24 μm (larger) is considered. The grain sizes are selected based on the significant size difference and the availability of temperature dependent thermoelectric properties in the existing literature. The power output is determined for different values of n and the results are put to comparative analysis. The same modelling framework, as given in Section "Modelling of the FGTED" of the present study, is employed.

Temperature dependent thermoelectric properties

The temperature dependent thermoelectric properties for the ZnO grains of sizes 0.18 ± 0.03 μm and 1.2 ± 0.24 μm are taken from an experimental research of Cramer et al.[45] The properties are curve fitted in Eqs. (22a), (22b), and (22c) for which the values of the coefficients (α, β, and γ) are as follows;

For 0.18 ± 0.03 μm ZnO grain size;

S_0 = -129.8250 μV/K, α_1 = 2.2261, α_2 = 1.3002, α_3 = -2.1676, κ_0 = 8.7343 W/m/K, β_1 = -0.1906, β_2 = -0.5644, β_3 = 0.5644, ρ_0 = 0.5358 Ω-m, γ_1 = -5.0122, γ_2 = 8.3177, γ_3 = -4.5172, T_0 = 375 K.

For 1.2 ± 0.24 μm ZnO grain size;

S_0 = -62.5644 μV/K, α_1 = -0.1960, α_2 = 1.6182, α_3 = 3.8257, κ_0 = 21.7749 W/m/K, β_1 = -0.7043, β_2 = 0.1358, β_3 = 0.0565, ρ_0 = 0.0512 Ω-m, γ_1 = -4.6705, γ_2 = 7.8686, γ_3 = -4.4721, T_0 = 375 K.

Using Eqs. (22a), (22b), (22c) and the values of the coefficients given in the present section, the S, κ, and ρ for the specified sizes of ZnO grains can be obtained at any temperature point in the range 375 K to 675 K.

Performance analysis

The temperature dependent thermoelectric properties for the S-FGTED with values of n in the range 0 to ∞, calculated using Eqs. (19a), (19b), and (19c), are represented in Fig. 14. The power outputs, determined employing the hybrid model described under section "Modelling of the FGTED", are represented in Fig. 15.

It can be observed from Fig. 15 that the minimum power output of 5.24 x 10^{-09} W is obtained when n = ∞ (homogeneous thermoelectric device composed entirely of 0.18 ± 0.03 μm sized ZnO grains). For n = 0.5, the power output obtained is 7.88 x 10^{-09} W. This represents a 50.38 % increase in power output as compared to n = ∞. The maximum power output of 4.12 x 10^{-08} W is obtained for n = 0 (homogeneous thermoelectric device composed entirely of 1.2 ± 0.24 μm sized ZnO grains). It can therefore be elucidated that the power output trend for S-FGTED is similar to that of the FGTED.

The thermoelectric properties for n = 0.5 lie consistently between those of n = 0 and n = ∞ across the entire temperature range, as given in Fig. 13. In particular, Fig. 14(a) and Fig. 14(b) shows that for n = 0 (homogeneous thermoelectric device composed entirely of ZnO grains sized 1.2 ± 0.24 μm), the S is lower and the κ is higher compared to other configurations. This observation appears to contradict the result of maximum power output being achieved for the homogeneous device composed entirely of larger grains. Notably, the ρ for the S-FGTED when n = 0 is significantly lower than that of S-FGTED with n = 0.5 and n = ∞ in the temperature range of 375 K to 650 K. This indicates that the influence of ρ on the power output is substantial enough to outweigh the adverse effects of lower S and higher κ.

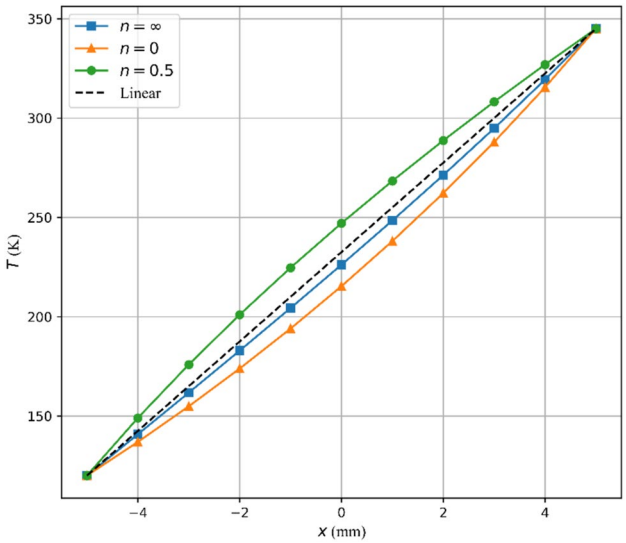

Fig. 13. Temperature distribution comparison for the FGTED. The current density (J) lies in the range 0 to 10000 A/m^2.

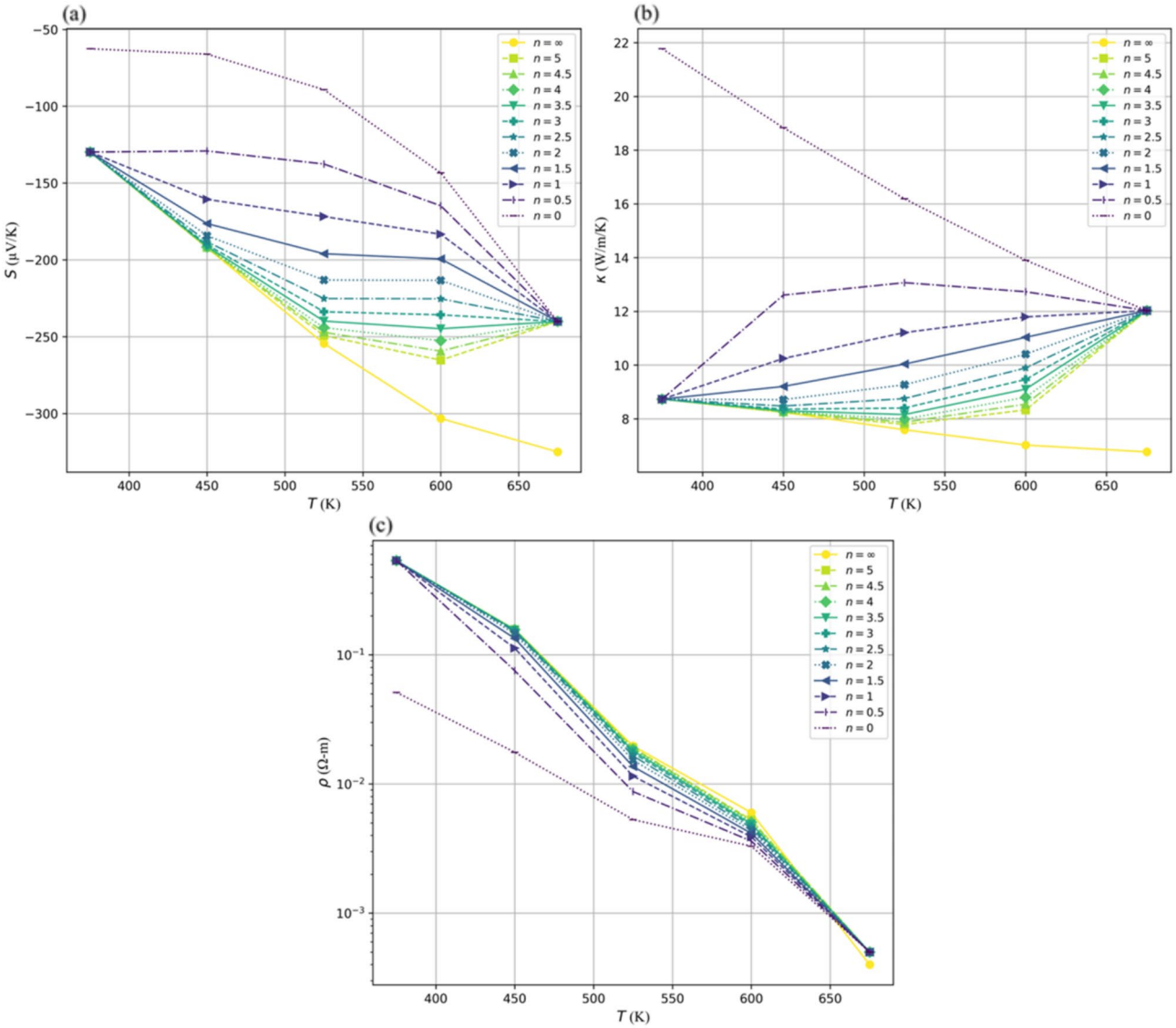

Fig. 14. Thermoelectric properties in the temperature range 375 K - 675 K for the S-FGTED composed of 0.18 ± 0.03 μm and 1.2 ± 0.24 μm sized ZnO grains; (**a**) *S*, (**b**) *κ*, (**c**) *ρ*.

The *ZT* vs. *T* and the *PF* vs. *T* curves for the S-FGTED when $n = 0$, 0.5, and ∞ (determined using Eq. (23) and Eq. (24)) are presented in Fig. 16(a) and Fig. 16(b), respectively. It can be elucidated from Fig. 16(a) that the *ZT* values for $n = \infty$, in the entire temperature range, is higher. This is mainly be due to the higher *S*, as shown in Fig. 14 (a), and also it being a squared term in *ZT* equation (Eq. (23)). When the *κ* is ignored, it can be observed from Fig. 16(b) that the *PF* in the temperature range 375 K - 450 K is higher for S-FGTED with $n = 0$. The *PF* in the 450 K - 675 K temperature range doesn't seems to vary much for the different *n* values. These observations further reinforce the indication that the major factor contributing to the highest power output in the S-FGTED with $n = 0$ is the *ρ*. To gain further clarity on this, a sensitivity analysis is performed in the subsequent section.

Sensitivity analysis

For the S-FGTED, the power output is maximum when $n = 0$ (larger grains), whereas the *ZT* is more for $n = \infty$ (smaller grains). Therefore, it is essential to examine the distinct contributions of the *S*, *κ*, and *ρ* to the power output. However, before carrying out the sensitivity analysis, it is essential to establish a method for determining the effective values of the thermoelectric properties along the length of the S-FGTED, as discussed in the subsequent section.

Effective values for the thermoelectric properties distribution

To determine the most suitable averaging method, the power outputs (of the S-FGTED having different values of *n*) obtained without any averaging approach are compared with those obtained using the averaged/effective values of the *S*, *κ*, and *ρ*. The effective/averaged values must be sufficiently accurate so that the power output

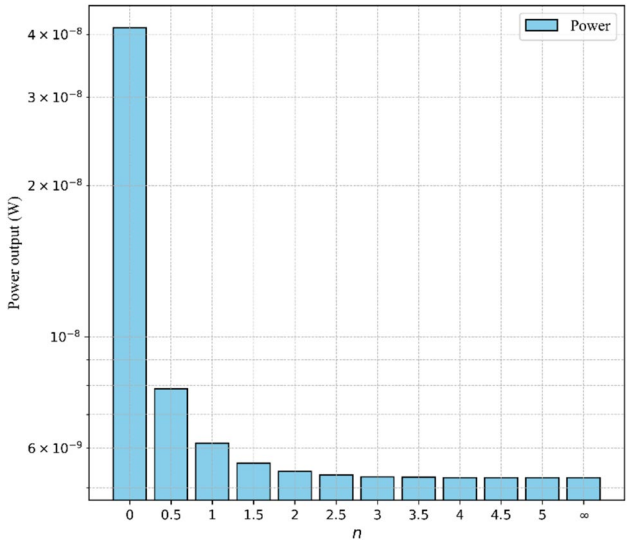

Fig. 15. Power output vs. n for S-FGTED composed of 0.18 ± 0.03 μm and 1.2 ± 0.24 μm sized ZnO grains. The cold and hot side temperature across the FGTED are 375 K and 675 K, respectively.

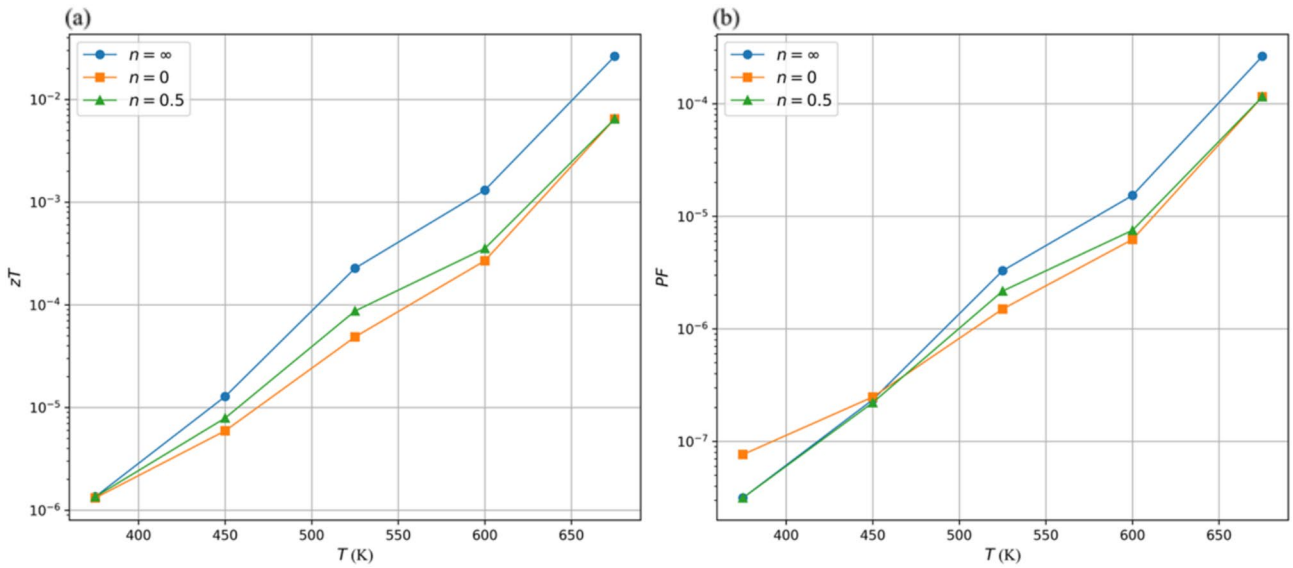

Fig. 16. Thermoelectric performance of the S-FGTED composed of 0.18 ± 0.03 μm and 1.2 ± 0.24 μm sized ZnO grains; (**a**) ZT vs. T curves, (**b**) PF vs. T curves.

calculated using them shows minimal deviation from that calculated using the original properties distribution[60]. The different averaging approaches employed are given as,

$$P_{seff.} = \frac{\sum_{i=1}^{N} P_i}{N}, \tag{26a}$$

$$P_{teff.} = P\left(T_m\right), \tag{26b}$$

where, P corresponds to the thermoelectric properties S, κ, and ρ. The subscript '$_i$' refers to the locations along the length of the S-FGTED, while N refers to the total number of locations. The subscript '$_m$' refers to the mean of the temperature range in which the device is operating. The subscripts '$_{seff.}$' and '$_{teff.}$' corresponds to the spatial and the temperature averaging methods, respectively.

A hybrid averaging method, in which the effective values for κ and ρ are calculated using Eq. (26a), while the effective value for S is calculated using Eq. (26b), is also employed. Fig. 17 represents the percentage relative

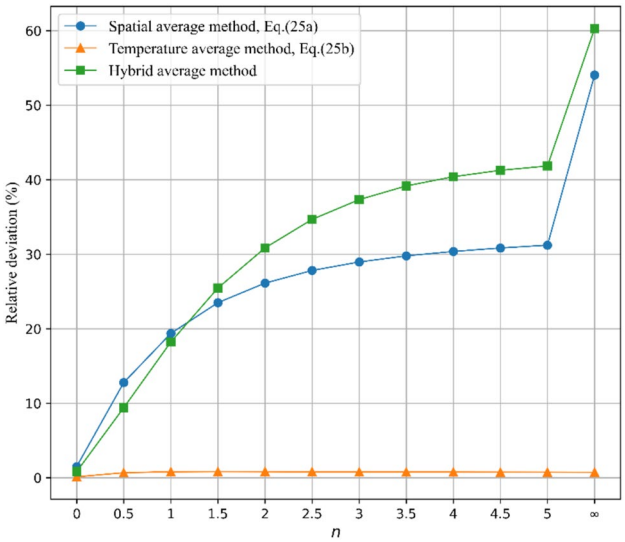

Fig. 17. Comparison of power outputs obtained using averaged thermoelectric properties with those obtained using original distribution of thermoelectric properties.

n	$S_{teff.}$ (μV/K)	$\kappa_{teff.}$ (W/m/K)	$\rho_{teff.}$ (Ω-m)	Power output (W)
0	89.1765	16.1923	0.0053	5.83×10^{-7}
0.5	137.5609	13.0692	0.0087	5.45×10^{-7}
1	171.8002	11.2114	0.0115	5.03×10^{-7}
1.5	195.9924	10.0386	0.0136	4.71×10^{-7}
2	213.1120	9.2703	0.0152	4.47×10^{-7}
2.5	225.2081	8.7546	0.0165	4.31×10^{-7}
3	233.7679	8.4030	0.0174	4.19×10^{-7}
3.5	239.8160	8.1605	0.0180	4.11×10^{-7}
4	244.0959	7.9920	0.0185	4.05×10^{-7}
4.5	247.1199	7.8743	0.0188	4.01×10^{-7}
5	249.2516	7.7918	0.0191	3.98×10^{-7}
∞	254.4239	7.5951	0.0197	3.91×10^{-7}

Table 4. Averaged values of the thermoelectric properties along with the obtained power outputs.

deviation between power outputs computed using the averaged/effective values of the S, κ, and ρ and those obtained from the original, non-averaged thermoelectric properties distribution. It can be observed from Fig. 17 that employing the temperature averaging method, given by Eq. (26b), results in the power output deviation of less than 2 % for the S-FGTED having values of n in the range 0 to ∞.

Sensivity analysis findings

To determine the most and the least significant thermoelectric property, a regression analysis is conducted using Minitab Statistical Software (version 3). A confidence level of 95 % is employed. The averaged/effective values of the thermoelectric properties (obtained using the temperature average method given in Eq. (26b)) for the S-FGTED with different n values and the corresponding power outputs are listed in Table 4. The analysis of variance (ANOVA) results obtained are listed in Table 5.

It can be elucidated from Table 5, that the P-value obtained is the least for the ρ and maximum for the κ. Therefore, it concludes that the power output is mostly affected by the ρ followed by the S, and lastly, the κ. Moreover, the R-squared value obtained is 99.91 %, which shows that the variation in power output (dependent variable) is very well explained by the variation in the thermoelectric properties (independent variable).

Conclusion

The present study provided a comprehensive analysis of the impact of spatial distribution of ZnO grains, of different sizes and in different volume fractions, on the power output of ZnO based FGTEDs. The developed analytical and computational hybrid framework effectively modelled and predicted the power output of the grain size graded ZnO based FGTEDs. The FDM combined with the Thomas algorithm provided accurate solution for

Source	DF	Adj SS	Adj MS	F-Value	P-Value
Regression	3	4.36×10^{-13}	0	1365255.44	0
$S_{teff.}$	1	0	0	1171.00	5.81×10^{-10}
$\kappa_{teff.}$	1	0	0	325.58	9.13×10^{-8}
$\rho_{teff.}$	1	0	0	2128.64	5.38×10^{-11}
Error	8	0	0		
Total	11	4.36×10^{-13}			

Table 5. ANOVA results.

the temperature distribution governing equation, enabling precise prediction of the temperature profiles. The spark plasma sintering method, combined with heat treatment, successfully fabricated ZnO samples of different grain sizes, achieving a high density of approximately 98%. Additionally, the sensitivity analysis accurately predicted the individual effects of the S, κ, and ρ on the power output. The findings revealed that:

1. The FGTEDs having higher volume fraction of larger ZnO grains generated higher power output.
2. The device composed of only 5.75 ± 0.06 μm sized ZnO grains produced the maximum power output of 2.6341×10^{-4} W. The maximum zT value of 0.006 is also obtained in the same device at 345 K.
3. The electrical resistivity (ρ) is observed to have the most significant effect on the power output, followed by the Seebeck coefficient (S) and the thermal conductivity (κ).
4. Optimizing grain size and its distribution can significantly enhance the performance of ZnO based FGTEDs.

ZnO as a thermoelectric material is highly stable at elevated temperatures. Therefore, the future research work in the domain could be exploring the effect of higher temperature, i.e., beyond 675 K, on the power output of ZnO based FGTEDs. Additionally, investigating the impact of alternate ZnO grain sizes could also be another promising direction.

Data availability

The author(s) confirm that the data supporting the findings of this study are available within the article.

Received: 25 July 2025; Accepted: 20 November 2025
Published online: 13 December 2025

References

1. Wu, Z., Zhang, S., Liu, Z., Mu, E. & Hu, Z. Thermoelectric converter: Strategies from materials to device application. *Nano Energy* **91**, 106692 (2022).
2. Tuoi, T. T. K., Van Toan, N. & Ono, T. Heat storage thermoelectric generator as an electrical power source for wireless Iot sensing systems. *Int. J. Energy Res.* **45**, 15557–15568 (2021).
3. Owais, M., Luo, X., Rehman, M., Mushtaq, R. T. & Alkahtani, M. Investigating Fe and Cr doping effects on thermoelectric efficiency in Mg3Sb2 through first-principles calculations for sustainable energy solutions. *Sci. Rep.* **15**, 9419 (2025).
4. Ding, G., Gao, G. & Yao, K. High-efficient thermoelectric materials: The case of orthorhombic IV-VI compounds. *Sci. Rep.* **5**, 9567 (2015).
5. Mahan, G., Sales, B. & Sharp, J. Thermoelectric materials: New approaches to an old problem. *Phys. Today* **50**, 42–47 (1997).
6. Rowe, D. M. *CRC Handbook of Thermoelectrics*. (CRC press, 2018).
7. Rosi, F. D. Thermoelectricity and thermoelectric power generation. *Solid. State. Electron.* **11**, 833–868 (1968).
8. Morgan, K. A. et al. High-throughput physical vapour deposition flexible thermoelectric generators. *Sci. Rep.* **9**, 4393 (2019).
9. Du, Y. et al. Thermoelectric fabrics: Toward power generating clothing. *Sci. Rep.* **5**, 6411 (2015).
10. Dresselhaus, M. S. et al. New directions for low-dimensional thermoelectric materials. *Adv. Mater.* **19**, 1043–1053 (2007).
11. Snyder, G. J. & Snyder, A. H. Figure of merit ZT of a thermoelectric device defined from materials properties. *Energy Environ. Sci.* **10**, 2280–2283 (2017).
12. Asfandiyar, C. B., Zhao, L. D. & Li, J. F. High thermoelectric figure of merit ZT> 1 in SnS polycrystals. *J. Mater.* **6**, 77–85 (2020).
13. Fang, W. et al. Monolayer SnX (X = O, S, Se): Two-dimensional materials with low lattice thermal conductivities and high thermoelectric figures of merit. *ACS Appl. Energy Mater.* **5**, 7802–7812 (2022).
14. Jin, Z.-H. Energy efficiency of thermoelectric materials: A three-dimensional study. *J. Appl. Phys.* **126**, (2019).
15. Tan, G., Ohta, M. & Kanatzidis, M. G. Thermoelectric power generation: From new materials to devices. *Philos. Trans. R. Soc. A Math. Phys. Eng. Sci.* **377**, 20180450 (2019).
16. Xiao, C., Li, Z., Li, K., Huang, P. & Xie, Y. Decoupling interrelated parameters for designing high performance thermoelectric materials. *Acc. Chem. Res.* **47**, 1287–1295 (2014).
17. Cao, X. S. & Yang, J. S. Analysis of thermoelectric generators with general material property variations. *J. Electron. Mater.* **48**, 5516–5522 (2019).
18. Cao, X., Niu, W., Cheng, Z. & Shi, J. Power series iterative approximation solution to the temperature field in thermoelectric generators made of a functionally graded temperature-dependent material. *J. Electron. Mater.* **49**, 5379–5390 (2020).
19. Jin, Z.-H., Wallace, T. T., Lad, R. J. & Su, J. Energy conversion efficiency of an exponentially graded thermoelectric material. *J. Electron. Mater.* **43**, 308–313 (2014).
20. Niu, W., Cao, X., Hu, Y., Wang, F. & Shi, J. Analytical analysis of temperature-dependent thermoelectric generator and optimization based on functionally graded materials. *Int. J. Energy Res.* **46**, 23963–23972 (2022).
21. Ju, C. et al. Performance analysis of a functionally graded thermoelectric element with temperature-dependent material properties. *J. Electron. Mater.* **48**, 5542–5554 (2019).
22. Banerjee, P. et al. Scalable and environmentally friendly MXene-tetrahedrites for next-generation flexible thermoelectrics. *J. Mater. Chem. A* **13**, 654–668 (2025).

23. Zabrocki, K., Müller, E. & Seifert, W. One-dimensional modeling of thermogenerator elements with linear material profiles. *J. Electron. Mater.* **39**, 1724–1729 (2010).
24. Müller, E., Drašar, Č, Schilz, J. & Kaysser, W. Functionally graded materials for sensor and energy applications. *Mater. Sci. Eng. A* **362**, 17–39 (2003).
25. Gelbstein, Y., Dashevsky, Z. & Dariel, M. P. Powder metallurgical processing of functionally graded p-Pb1−xSnxTe materials for thermoelectric applications. *Phys. B Condens. Matter* **391**, 256–265 (2007).
26. Dashevsky, Z., Shusterman, S., Dariel, M. P. & Drabkin, I. Thermoelectric efficiency in graded indium-doped PbTe crystals. *J. Appl. Phys.* **92**, 1425–1430 (2002).
27. Belmonte, M., Gonzalez-Julian, J., Miranzo, P. & Osendi, M. I. Continuous in situ functionally graded silicon nitride materials. *Acta Mater.* **57**, 2607–2612 (2009).
28. Banerjee, P. et al. Effect of particle-size distribution and pressure-induced densification on the microstructure and properties of printable thermoelectric composites and high energy density flexible devices. *Nano Energy* **89**, 106482 (2021).
29. Mahan, G. D. Inhomogeneous thermoelectrics. *J. Appl. Phys.* **70**, 4551–4554 (1991).
30. Jin, Z.-H. & Wallace, T. T. Functionally graded thermoelectric materials with arbitrary property gradations: A one-dimensional semianalytical study. *J. Electron. Mater.* **44**, 1444–1449 (2015).
31. Ju, C., Dui, G., Zheng, H. H. & Xin, L. Revisiting the temperature dependence in material properties and performance of thermoelectric materials. *Energy* **124**, 249–257 (2017).
32. Kim, H. S., Liu, W., Chen, G., Chu, C.-W. & Ren, Z. Relationship between thermoelectric figure of merit and energy conversion efficiency. *Proc. Natl. Acad. Sci.* **112**, 8205–8210 (2015).
33. Sulaiman, S., Sudin, I., Al-Naib, U. M. B. & Omar, M. F. Review of the nanostructuring and doping strategies for high-performance ZnO thermoelectric materials. *Crystal* **12**, 1076 (2022).
34. Yu, L. & Skov, A. L. ZnO as a cheap and effective filler for high breakdown strength elastomers. *RSC Adv.* **7**, 45784–45791 (2017).
35. Ali, A., Phull, A.-R. & Zia, M. Elemental zinc to zinc nanoparticles: Is ZnO NPs crucial for life? Synthesis, toxicological, and environmental concerns. *Nanotechnol. Rev.* **7**, 413–441 (2018).
36. Park, Y., Cho, K. & Kim, S. Thermoelectric characteristics of glass fibers coated with ZnO and Al-doped ZnO. *Mater. Res. Bull.* **96**, 246–249 (2017).
37. Singh, D. J. & Terasaki, I. Nanostructuring and more. *Nat. Mater.* **7**, 616–617 (2008).
38. Ge, B., Li, R., Wang, G., Zhu, M. & Zhou, C. Oxide semiconductors for thermoelectric: The challenges and future. *J. Am. Ceram. Soc.* **107**, 1985–1995 (2024).
39. Nam, W. H., Lim, Y. S., Choi, S.-M., Seo, W.-S. & Lee, J. Y. High-temperature charge transport and thermoelectric properties of a degenerately Al-doped ZnO nanocomposite. *J. Mater. Chem.* **22**, 14633 (2012).
40. Gautam, D. et al. Thermoelectric properties of pulsed current sintered nanocrystalline Al-doped ZnO by chemical vapour synthesis. *J. Mater. Chem. A* **3**, 189–197 (2015).
41. Ohtaki, M., Araki, K. & Yamamoto, K. High thermoelectric performance of dually doped ZnO Ceramics. *J. Electron. Mater.* **38**, 1234–1238 (2009).
42. Tang, J. et al. Holey silicon as an efficient thermoelectric material. *Nano Lett.* **10**, 4279–4283 (2010).
43. Yang, L., Yang, N. & Li, B. Extreme Low thermal conductivity in nanoscale 3D Si phononic crystal with spherical pores. *Nano Lett.* **14**, 1734–1738 (2014).
44. Sulaiman, S., Izman, S., Uday, M. B. & Omar, M. F. Review on grain size effects on thermal conductivity in ZnO thermoelectric materials. *RSC Adv.* **12**, 5428–5438 (2022).
45. Cramer, C. L., Gonzalez-Julian, J., Colasuonno, P. S. & Holland, T. B. Continuous functionally graded material to improve the thermoelectric properties of ZnO. *J. Eur. Ceram. Soc.* **37**, 4693–4700 (2017).
46. Cramer, C. L. *et al.* Testing and modeling of functionally graded aluminum-doped zinc oxide using spark plasma sintering and discrete powder layers of varying composition. *Phys. status solidi* **219**, (2022).
47. Rai, S., Tewari, A. & Gupta, A. A novel mathematical model for porosity-dependent thermoelectric properties in Al-Doped ZnO functionally graded devices: Performance analysis and optimization. *J. Electron. Mater.* **54**, 8593–8609 (2025).
48. Hammer, P. C. Finite-difference methods for partial differential equations. *Technometrics* **4**, 143–144 (1962).
49. Aziz, A. A., Afriza, N., Baki, B. & Pengkomputeran, K. P. Application of finite difference method(fdm) and finite element method(fem) in solving heat problem. **15**, 11–16 (2024).
50. Skiba, Y. N. A non-iterative implicit algorithm for the solution of advection–diffusion equation on a sphere. *Int. J. Numer. Methods Fluids* **78**, 257–282 (2015).
51. Quesada-Barriuso, P., Lamas-Rodríguez, J., Heras, D. B., Bóo, M., & Argüello, F. Selecting the best tridiagonal system solver projected on multi-core CPU and GPU platforms. In *Proc. International Conference on Parallel and Distributed Processing Techniques and Applications (PDPTA)* 1 (2011).
52. Gupta, A. & Talha, M. Recent development in modeling and analysis of functionally graded materials and structures. *Prog. Aerosp. Sci.* **79**, 1–14 (2015).
53. Lide, D. R. *CRC Handbook of chemistry and physics*. vol. 84 (CRC press, 2004).
54. Jaegle, M. Multiphysics simulation of thermoelectric systems - Modeling of peltier-cooling and thermoelectric generation. *COMSOL Conf. 2008 Hann.* 7 (2008).
55. Mayandi, J. et al. Al-doped ZnO prepared by co-precipitation method and its thermoelectric characteristics. *Mater. Lett.* **288**, 129352 (2021).
56. Himabindu, B., Latha Devi, N. S. M. P., Nagaraju, P. & Rajini Kanth, B. A nanostructured Al-doped ZnO as an ultra-sensitive room-temperature ammonia gas sensor. *J. Mater. Sci. Mater. Electron.* **34**, 1014 (2023).
57. Rahaman, M. N. *Ceramic Processing and Sintering*. (CRC Press, 2017). https://doi.org/10.1201/9781315274126.
58. Wu, X. et al. Thermal conductivity of Wurtzite Zinc-oxide from first-principles lattice dynamics – a comparative study with gallium nitride. *Sci. Rep.* **6**, 22504 (2016).
59. Mehdizadeh Dehkordi, A., Zebarjadi, M., He, J. & Tritt, T. M. Thermoelectric power factor: Enhancement mechanisms and strategies for higher performance thermoelectric materials. *Mater. Sci. Eng. R. Rep.* **97**, 1–22 (2015).
60. Ponnusamy, P., de Boor, J. & Müller, E. Using the constant properties model for accurate performance estimation of thermoelectric generator elements. *Appl. Energy* **262**, 114587 (2020).

Acknowledgements

We acknowledge the support received for this project under the Core Research Grant CRG/2022/006689 from the Anusandhan National Research Foundation (ANRF), India. We also extend our gratitude to the Indian Institute of Technology, Roorkee and the Shiv Nadar Institution of Eminence for providing financial assistance and other essential resources necessary for the successful execution of this project.

Author contributions

Shardul Rai: Conceptualization, Writing – original draft. Kshitij Kumar Sharma: Conceptualization, experimentation Abhishek Tewari: Writing – review & editing, Conceptualization, Supervision Ankit Gupta: Writing – re-

view & editing, Supervision, Conceptualization.

Funding
Open access funding provided by Shiv Nadar University. Anusandhan National Research Foundation (ANRF), CRG/2022/006689

Declarations

Competing interests
The authors declare no competing interests.

Additional information
Correspondence and requests for materials should be addressed to A.G.

Reprints and permissions information is available at www.nature.com/reprints.

Publisher's note Springer Nature remains neutral with regard to jurisdictional claims in published maps and institutional affiliations.